Autocatalytic model of oscillatory zoning in experimentally grown $(Ba,Sr)SO_4$ solid solution

Sergei Katsev and Ivan L'Heureux*
Ottawa-Carleton Institute for Physics, University of Ottawa, 150 Louis Pasteur, Ottawa, Ontario, Canada K1N 6N5
(Received 25 July 2002; published 12 December 2002)

Oscillatory zoning (OZ) is a phenomenon common to many natural minerals whereby the mineral composition varies more or less regularly from the core of the crystal to its rim. Oscillatory zoned barite-celestite $(Ba,Sr)SO_4$ crystals are one of the very few examples of the OZ phenomenon that were obtained under controlled laboratory conditions. It is known that such crystals can be synthesized by precipitation from an aqueous solution during counterdiffusion in a gel column connecting two reservoirs. We present here a model of oscillatory zoning in such a binary solid solution grown from an aqueous solution. By expanding on a previously suggested model, we obtain oscillatory dynamical solutions for two limit cases: the growth of a flat crystal face and the growth of a spherical crystallite. We consider an autocatalytic dependence between the crystal growth rate and the crystal surface composition. The oscillatory patterns then arise as a kinetic effect due to the coupling between the diffusion field around the crystal and the fast crystal growth under far-from-equilibrium conditions. The effects of fluctuations in the aqueous solution concentrations are also considered. It is shown that they may lead to noisy oscillatory patterns.

DOI: 10.1103/PhysRevE.66.066206 PACS number(s): 47.54.+r, 81.10.Aj, 05.65.+b, 91.60.Hg

I. INTRODUCTION

Many minerals exhibit oscillatory zoning, whereby the composition varies inside the crystals in a nonmonotonic fashion in the direction from the crystal core to its rim. For a long time, oscillatory zoning was believed to be a rare phenomenon, an anomalous case of mineral zoning. However, with the development of more sophisticated observation techniques, it was shown that such zoning, in one form or another, is found in many mineral classes and in a wide range of geological environments [1]. Understanding the origin of the zoning is important, as it may provide information on the genesis of the mineral and the geological history of its host rock. For instance, in hydrothermal environments, it may yield insights into the details of fluid-rock interactions.

In many minerals, oscillatory patterns reflect variations in the geological environment at the time of mineral formation (so-called extrinsic mechanism). However, other mechanisms are possible. It is known that spatiotemporal patterns can arise spontaneously without external templates in nonlinear systems subjected to far-from-equilibrium conditions (intrinsic mechanism). In particular, reaction-diffusion systems have long since been known to hold potential for self-organization [2]. In the case of crystal growth under conditions far-from-thermodynamic equilibrium, a fast crystal growth rate may provide nonlinear couplings between different dynamical variables, which is a necessary condition for self-organization.

In spite of widespread observations of oscillatory zoning and a relative abundance of theoretical models used to explain the pattern formation in various environments, the zoning patterns have almost never been obtained under controlled laboratory conditions in crystal nucleation and growth experiments. One of the very few examples of mineral oscillatory zoning that have been reproduced in a laboratory are the oscillatory patterns in the solid solution of barite $(BaSO_4)$ and celestite $(SrSO_4)$ synthesized by Putnis's group [3]. Oscillatory zoned single crystals of barite celestite contained up to ten zones, whereby Ba crystal composition switched abruptly between roughly 25% and 90%. The typical zone width was about 7–10 μm and the typical zoned crystallites were about 150 μm in size.

In a series of experiments by Putnis's group [3–6], barite and barite-celestite solid solution crystals were grown from an aqueous solution during counterdiffusion in a gel column connecting two reservoirs containing the initial reactants (Fig. 1). One month after the start of the experiment, the crystals were extracted from the gel and their morphology was studied by scanning electron microscopy. Various zoning textures [4] corresponding to different initial reservoir concentrations are listed here in Table I.

The experiment was conducted in a controlled environment and therefore many of the microscopic crystal growth parameters are known or can be estimated with sufficient precision. Nucleation and growth of the $(Ba,Sr)SO_4$ crystals from an aqueous solution have been extensively studied

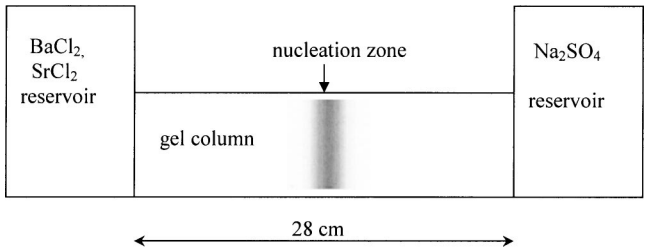

FIG. 1. Experimental setup, in which oscillatory zoned crystals of $(Ba,Sr)SO_4$ were synthesized in Ref. [3]. The reservoirs containing the mother solutions are connected by a gel column 28 cm in length. The reactants counterdiffuse in the column and $(Ba,Sr)SO_4$ crystals nucleate and grow in some region (shown as gray) inside the column. After a month of growth, the crystals were extracted and their morphology was studied by scanning electron microscopy.

*Corresponding author. Email address: ilheureu@physics.uottawa.ca

TABLE I. Experimentally obtained textures in $(Ba,Sr)SO_4$. The crystal zoning experimental data are taken from Ref. [4]. The nucleation time is counted from the moment the solutions enter the gel column. Zoning type notation: OZ=oscillatory zoning, $Z1$=Ba-Sr-Ba, BA=barite, Z2=Sr-Ba-Sr.

Concentrations at the reservoirs M_i, M $Ba/Sr/SO_4$	Type of zoning	Nucleation location[a] y, cm	Core[b] composition X	Nucl. time τ, h	Concentration at nucleation,[c] $\hat{m}$, mM $Ba/Sr/SO_4$
0.5/0.5/0.5	OZ	13–16	0.90	288	7.7-1.4/6.8-1.2/1.4-8.7
0.5/0.5/0.3	OZ	15–18	0.90	312	3.6-0.6/3.1-0.5/4.0-17.1
0.3/0.3/0.5	OZ	16[d]	0.91	336	1.7/1.6/13[d]
0.3/0.3/0.3	$Z1$	13–15		360	9.0-3.7/8.2-3.2/2.4-6.4
0.5/0.5/0.1	$Z1$	17–20	0.88	384	3.0-0.6/2.6-0.5/5.9-17.0
0.3/0.3/0.1	$Z1$	18[d]	0.89	408	1.6/1.4/24[d]
0.3/0.1/0.1	*BA*	21[d]	0.94	576	1.7/0.8/30[d]
0.1/0.3/0.1	$Z1$ and $Z2$	21[d]	0.79	624	0.9/1.6/31[d]

[a]Location of the nuclei in the gel column is taken from Ref. [5], where it was reported for the pure barite case.

[b]The composition of the crystal core is assumed equivalent to the composition of the newly nucleated crystallites. The corresponding data are taken from Ref. [6].

[c]The concentrations at the nucleation site were calculated from Eq. (16). The range of the values given corresponds to the range in the nucleation location y.

[d]The concentrations of Ba^{2+} and Sr^{2+} at the nucleation site at the nucleation time were taken from Ref. [4]. The corresponding nucleation location and the concentration of $SO_4{}^{2-}$ were calculated using Eq. (16).

[5–8] and data are available for many of the important parameters. Since the detailed information about the crystal growth environment is almost never available for natural minerals, constructing a model that would simulate the experimentally observed oscillatory zoning is an important step towards understanding natural oscillatory zoning.

In this paper, we suggest an autocatalytic model of oscillatory banding in $(Ba,Sr)SO_4$ crystals, which extends the previously suggested model of L'Heureux and Jamtveit [9]. In that work, the autocatalytic crystal growth of a flat crystallite surface and the diffusion of the components in the solution around the crystal were described in terms of partial differential equations (PDEs). The model was then reduced to a set of ordinary differential equations (ODEs) by introducing a boundary layer approximation. Linear stability analysis of those equations and their direct numerical solution demonstrated the existence of oscillatory solutions. Here, the numerical solutions to the original set of PDEs are obtained for two limit cases: the one-dimensional growth of a flat crystal face and the growth of a small spherical crystallite. Also, a reduced model for the growth of a spherical crystallite is considered, which allows us to perform a more complete linear stability analysis. The effects of fluctuations in the crystal growth environment on the oscillatory pattern formation are also considered in this paper. Although the specific case of $(Ba,Sr)SO_4$ is illustrated here, the mechanisms described in this paper are general and could be applied to other solid solutions grown from an aqueous solution.

In our model, the oscillatory solutions are obtained as a result of nonlinear coupling between the kinetics of the molecular attachment processes at the crystal-solution interface and the diffusion field around the crystal. In the approximation of a spherical crystallite, the onset of oscillations is related to the transition from an interface-controlled crystal growth regime to a diffusion-controlled growth, which occurs as the crystallite size increases. In addition, reasonably small fluctuations in the bulk concentrations of the components are shown to facilitate large-magnitude dynamic transitions between the compositional ranges and thus enlarge the parameter range in which oscillatory zoning can be achieved.

The paper is organized as follows. First, the model is presented and its steady-state solutions are discussed. Then the numerical results are presented. After that, the model is reduced to a set of ODEs in the approximation of a spherical crystallite and a linear stability analysis of the resulting system of equations is performed. The reduced system is then solved numerically. Finally, the effect of noise on the full PDE model is considered and the results are summarized. An appendix completes the paper.

II. MODEL

We consider the growth of $(Ba,Sr)SO_4$ crystals from a solution in the setup shown in Fig. 1. We are not interested in the nucleation phase [8] and therefore consider only the growth process for a previously nucleated crystallite. The growth proceeds according to the precipitation reactions

$$SO_4{}^{2-} + Ba^{2+} \rightarrow BaSO_4, \quad SO_4{}^{2-} + Sr^{2+} \rightarrow SrSO_4,$$

where both $BaSO_4$ and $SrSO_4$ are incorporated in the same crystal to form a solid solution. The following symbolic notation is used in the description of the model below:

$A=SO_4^{2-}$, $B=Ba^{2+}$, $C=Sr^{2+}$, $BA=BaSO_4$, and $CA=SrSO_4$. Since the growth layers of similar chemical composition in the observed zoned crystals are parallel to the crystal faces, we first consider growth only in one dimension, in the direction perpendicular to the crystal face. We choose a frame of reference moving with the growing crystal in such a way that $x=0$ always corresponds to the crystal-solution interface. Thus, $x>0$ corresponds to the space occupied by the aqueous solutions, whereas $x<0$ is associated with the space occupied by the crystal.

If $m_i(x,t)$ are the concentrations (moles per volume) of the ions of species i ($i=A$, B, or C) and V is the rate of the crystal surface advance (length/time) then the evolution of the species concentration fields in the diffusion boundary layer surrounding the crystal is given by the diffusion equations

$$\frac{\partial m_i}{\partial t}=D_i\frac{\partial^2 m_i}{\partial x^2}+V\frac{\partial m_i}{\partial x}, \tag{1}$$

where D_i are the diffusion coefficients in the solution (assumed independent of the concentration) and the second term is due to the choice of the coordinate system. The boundary condition far from the growing crystal is naturally given by

$$m_i(\infty,t)=\hat{m}_i(t) \tag{2}$$

where $\hat{m}_i(t)$ are the bulk values of the concentrations at the crystallization site that may depend on time due to the influx of species from the reservoirs. In the experiments of Refs. [3–6], the size of the grown barite-celestite crystallites was always much smaller than the dimensions of the gel column (1.2 cm in diameter, 28 cm in length). Therefore, the solution in the gel at the nucleation site can be considered to have, locally, the same bulk species concentrations in all directions around the crystallite. The continuity of the mass current at the crystal-solution interface ($x=0$) gives the second boundary condition:

$$D_i\frac{\partial m_i}{\partial x}\bigg|_{x=0}+[m_i(0,t)-c_i(t)]V=0, \tag{3}$$

where $c_i(t)$ denotes the molar concentration in the solid at the growing front. It is clear from the stoichiometry that $c_A=c_B+c_C$. Also, for the case of crystal growth from a solution, $c_i\gg m_i$.

Since the above estimates suggest that a change in the growth mechanism may occur as the crystal becomes larger, an extension of the model to the case of a spherical crystal is useful. By writing the diffusion equations for the species in the solution in spherical coordinates and assuming growth in the radial direction only, equations (1), (2), and (3) can be transformed into

$$\frac{\partial m_i}{\partial t}=D\frac{\partial^2 m_i}{\partial \rho^2}+\frac{2D}{\rho'}\frac{\partial m_i}{\partial \rho}+V\frac{\partial m_i}{\partial \rho}, \tag{4}$$

$$m_i(\rho\to\infty,t)=\hat{m}_i(t), \tag{5}$$

$$D\frac{\partial m_i}{\partial \rho}\bigg|_{\rho=0}+[m_i(0,t)-c_i(t)]V=0, \tag{6}$$

where ρ is the distance from the interface measured in the radial direction and ρ' is the distance from the center of the crystal. If the initial nucleus has the size r_0, then

$$\rho'(t)=\rho(t)+r_0+\int_0^t V(t')dt'. \tag{7}$$

It is convenient to describe the composition of the solid phase by the mole fraction of $BaSO_4$ in the crystal $X(0\leqslant X\leqslant 1)$. The relationship between X and c_i is then given by

$$c_B=\frac{X}{v_{BA}X+v_{CA}(1-X)},\quad c_C=\frac{1-X}{v_{BA}X+v_{CA}(1-X)}, \tag{8}$$

where v_{BA} and v_{CA} are the molar volumes of the solid $BaSO_4$ and $SrSO_4$, respectively.

The evolution of the crystal composition X at the interface is determined kinetically by the rates V_{BA} and V_{CA} at which the units of *BA* and *CA* are attached (or detached) to the crystal surface. They can be defined as the rate of growth of a flat crystal face consisting of pure $BaSO_4$ and $SrSO_4$, respectively, in meter per second. The total growth velocity is then [9]

$$V=V_{BA}+V_{CA}. \tag{9}$$

As argued in Ref. [9], it is useful to introduce another equation that describes the dynamics of the composition X across the crystal-solution interface. Using mass balance across that interface and assuming normal crystal growth mechanism, we obtain (see the Appendix)

$$L\alpha\frac{dX}{dt}=[V_{BA}-X(V_{BA}+V_{CA}/\alpha)][X+(1-X)\alpha]^2, \tag{10}$$

where $\alpha=v_{CA}/v_{BA}=0.89$ and L is the effective crystal-solution interface width which characterizes the roughness of the interface. If the difference in molar volume is neglected, this equation reduces to

$$L\frac{dX}{dt}=V_{BA}-XV. \tag{11}$$

In the steady state, the crystal composition is thus kinetically defined [10] as $X=V_{BA}/V$.

The three equations (1) or (4) are coupled among themselves as well as with Eq. (10) through the term containing the growth velocity V.

In general, the crystal growth rate V depends nonlinearly on the concentrations in the solution m_A, m_B, and m_C near the interface. In the case of a continuous two-component growth of the crystal surface in contact with a dilute solution, the growth rate can be approximated by

$$V_{BA}=\beta'_{BA}(m_Bm_A-m_B^0m_A^0), \tag{12}$$

where m_i^0 are the equilibrium concentrations in the solution and β'_{BA} is the kinetic coefficient [11]

$$\beta'_{BA}=a_{BA}fv_{BA}^2(a_{BA}/\delta_{BA})^2\exp[-\Delta U_{BA}/kT]. \quad (13)$$

Here, a_{BA} is the size of a molecular building unit, f is a frequency factor, v_{BA} is the molar volume in the solid, δ_{BA} is the average distance between kink sites on the growing surface, and ΔU_{BA} is the energy barrier for the incorporation of the building unit into the crystal. The factor $(a_{BA}/\delta_{BA})^2$ characterizes the probability of finding a suitable kink site on the two-dimensional surface of the crystal. The growth rate V_{CA} can be defined in a similar way.

Attachment of the $BaSO_4$ units to the $BaSO_4$ kink sites is energetically favored over their attachment to the $SrSO_4$ kink sites because of the lattice misfit and because chemical bonding is generally stronger between units of the same species. Thus the average distance between the favorable kink sites for the attachment of $BaSO_4$ is expected to decrease with increasing $BaSO_4$ molar fraction in the crystal surface. The simplest relation that mimics this dependence on the crystal composition is [9]

$$(a_{BA}/\delta_{BA})\propto X+p_1, \quad (a_{CA}/\delta_{CA})\propto 1-X+p_2, \quad (14)$$

where the constants $p_{1,2}$ characterize the residual probabilities of finding a favorable kink site for the growth of $BaSO_4$ on a pure $SrSO_4$ surface, and vice versa. The growth rates then take the form

$$V_{BA}=\beta_{BA}(m_Bm_A-m_B^0m_A^0)(X+p_i)^2,$$

$$V_{CA}=\beta_{CA}(m_Cm_A-m_C^0m_A^0)(1-X+p_2)^2, \quad (15)$$

where $\beta_{BA,CA}$ are new kinetic coefficients. For highly supersaturated solutions, the product of the equilibrium concentrations in Eqs. (15) can be neglected [9]. This expression for the growth rates thus describes the autocatalytic growth of a two-component crystal.

The autocatalytic dependence of the growth rates on the crystal composition provides the possibility of generating oscillatory patterns in the crystal composition by the following qualitative mechanism. When the surface of a growing crystallite is rich in, say, *B*, the attachment of *B* units to the crystal surface from the solution is energetically favored over the attachment of *C*. Thus, a *B*-rich crystal zone is formed while the solution in the vicinity of the crystal is being depleted of *B* and becomes enriched in *C*. Eventually, a *C*-rich layer will nucleate on the surface of the *B*-rich crystal, which causes further autocatalytic attachment of the *C* units from the solution and therefore a growth of a *C*-rich crystal zone. This, in turn, depletes the solution of *C* while diffusion gradually increases the concentration of *B* until nucleation of *B* occurs and the cycle is thus repeated.

To correctly simulate the crystal growth experiment in the setup shown in Fig. 1, it is necessary to know the time dependence of the bulk concentrations $\hat{m}_i$ in the solution at the crystallization site. The evolution of the concentration profiles in the gel can be found analytically [9] by solving the corresponding diffusion equations. Considering the reservoirs to be inexhaustible (which is a good approximation for the experiment duration times smaller than one month and for large reservoir concentrations [5]) and neglecting the depletion of the solution due to crystallization, the time evolution of the aqueous concentrations at the crystallization site is given by

$$\hat{m}_{B,C}(t)=M_{B,C}\,\mathrm{erfc}\left(\frac{y}{2\sqrt{D_{B,C}(t+\tau)}}\right),$$

$$\hat{m}_A(t)=M_A\,\mathrm{erfc}\left(\frac{H-y}{2\sqrt{D_A(t+\tau)}}\right), \quad (16)$$

where M_i are the known concentrations of the components i in the reservoir; y is the distance from the $BaCl_2$-$SrCl_2$ reservoir to the nucleation site; $H=28$ cm is the total column length; and τ is the nucleation time measured from the moment the solutions enter the gel column. The location of the crystallization site y can be determined from the $BaSO_4$-$SrSO_4$ nucleation experiments in the same experimental setup [5,6].

Equations (1) with the boundary conditions (2) and (3) do not have a steady-state solution. This is easily shown by tentatively setting the left-hand side of the equation to zero and integrating twice over the space coordinate x to obtain what would be the steady-state concentration distribution in the solution,

$$m_{\mathrm{st}_i}(x)=C_{1i}+\frac{D_i}{V}\exp\left(-\frac{x}{D_i/V}\right)C_{2i}. \quad (17)$$

The integration constant C_{1i} can be obtained from the boundary condition (2):

$$C_{1i}=\hat{m}_i. \quad (18)$$

The boundary condition (3) does not allow the determination of the second integration constant C_{2i} but leads to $\hat{m}_i=c_{\mathrm{st}_i}$, where c_{st_i} are the steady-state molar concentrations in the crystal. The latter relation is impossible to satisfy for both Ba and Sr at the same time because the concentration in the solid phase c_{st} is always greater than the corresponding concentration in the aqueous solution $\hat{m}$ for at least one of these species.

A steady state may be achieved, however, if a diffusion boundary layer of finite width is considered. If the boundary condition (2) is taken not at infinity but at some finite distance from the interface l, then the integration constant C_{2i} can be obtained as

$$C_{2i}=\frac{V}{D_i}(\hat{m}_i-c_{\mathrm{st}_i})e^{(V/D_i)l} \quad (19)$$

and equation (17) becomes

$$m_{\mathrm{st}_i}(x)=c_{\mathrm{st}_i}-(c_{\mathrm{st}_i}-\hat{m}_i)e^{(V/D_i)l}. \quad (20)$$

By taking this relation at $x=0$ and expanding the exponent, the boundary layer width can be obtained as

$$l=\frac{D_i}{V}\frac{\hat{m}_i-m_i(0)}{c_{\mathrm{st}_i}-\hat{m}}\approx\frac{D_i}{V}\frac{\hat{m}_i-m_i(0)}{c_{\mathrm{st}_i}}. \tag{21}$$

In this case, the concentration profiles in the solution near the crystal interface have an approximately linear form,

$$m_i(x)\approx m_i(0)+c_{\mathrm{st}_i}\frac{V}{D_i}x. \tag{22}$$

While the current work does not rely on the above simplifications, the approximations (21) and (22) were taken in Ref. [9].

If, instead of linear growth in one dimension, the radial growth of a spherical crystallite is considered, then a pseudo-steady-state solution can be obtained. If the diffusion field in the solution adjusts itself adiabatically quickly to the changes caused by the increase in the crystal size and the difference in solid molar volume is neglected so that $X_{\mathrm{st}}=V_{BA}/V$ in eq. (11), a pseudo-steady-state concentration profile in the solution can be obtained in the form

$$m_i(\rho')\approx\hat{m}_i-\frac{V_i}{vD_i}\frac{r^2}{\rho'}, \tag{23}$$

where the steady-state growth rate V_i is either $V_B=V_{BA}$ or $V_C=V_{CA}$ or $V_A=V_{BA}+V_{CA}$, r is the slowly increasing crystal radius, $\rho'\geqslant r$ is the distance from the center of the crystal, and v is the molar volume. When the second term is small, the concentration near the crystal-solution interface is close to the bulk concentration value and the crystal growth occurs in the kinetic regime. However, as the crystal becomes larger, diffusion starts to play a role.

The pseudo-steady-state concentrations at the interface $m_i(r)$ are obtained as the solution of the system of equations (23) taken at $\rho'=r$ where the growth rates V_i depend on $m_i(r)$ through (15). If the solution concentration at the interface is not very different from its bulk value and the equilibrium concentrations in Eqs. (15) are neglected then the steady-state concentrations at the interface are

$$\begin{aligned} m_A&\approx\hat{m}_A[1-\hat{m}_B\alpha'_B-\hat{m}_C\alpha'_C]\\ m_B&\approx\hat{m}_B[1-\hat{m}_A\alpha_B],\\ m_C&\approx\hat{m}_C[1-\hat{m}_A\alpha_C], \end{aligned} \tag{24}$$

where

$$\alpha_B=r\frac{1}{v}\beta_{BA}(X+p_1)^2/D_B,$$

$$\alpha_C=r\frac{1}{v}\beta_{CA}(1-X+p_2)^2/D_C,$$

$$\alpha'_B=r\frac{1}{v}\beta_{BA}(X+p_1)^2/D_A,\quad \alpha'_C=r\frac{1}{v}(1-X+p_2)^2/D_A.$$

In the general case of arbitrary interface concentrations, the pseudo-steady-state solution also exists and is continuous both in r and X, as verified numerically for a wide range of parameter values. This indicates that, under the current approximations, the steady-state solution is always stable. Therefore, oscillatory solutions or switching between steady states are only possible when those approximations cease to be valid, i.e., when the distortion of the diffusion field in the solution due to the changes in the crystal size r is considered.

The pseudo-steady-state value of the composition X is obtained by setting the left-hand side of the Eq. (11) equal to zero. Using the approximation (15) one obtains

$$X_{\mathrm{st}}=\frac{V_{BA}}{V}=\frac{\beta_{BA}m_B(X_{\mathrm{st}}+p_1)^2}{\beta_{BA}m_B(X_{\mathrm{st}}+p_1)^2+\beta_{CA}m_C(1-X_{\mathrm{st}}+p_2)^2}. \tag{25}$$

If the concentrations m_B and m_C are similar, $\beta_{BA}\approx\beta_{CA}$, and the small parameters p_1 and p_2 are approximately equal, then the pseudo-steady-state composition is close to one of the values in the set

$$X^*=\{0,\ 0.5,\ \text{or}\ \ 1\}. \tag{26}$$

These values correspond to pure $SrSO_4$, a crystal composition with equal proportions of Ba and Sr sulphate, or pure $BaSO_4$, respectively.

The diffusion of the Ba^{2+}, Sr^{2+}, and $SO_4{}^{2-}$ ionic species in the gel is complicated by the electric interactions between the ions in the solution. Far from the nucleation zone, the binary salt diffusion from the reservoirs (Fig. 1) may be characterized by the diffusion coefficients computed from the Nernst-Hartley relation

$$D_{\mathrm{salt}}=\frac{(z_++|z_-|)D_+D_-}{z_+D_++|z_-|D_-}, \tag{27}$$

where D_+ and D_- are the tracer diffusion coefficients for the cations and anions and z_+ and z_- are the respective charges. The overall electroneutrality of the solution is maintained by the coupling between the cation and anion diffusions. Using ionic diffusion data for individual elements [12], the binary diffusion coefficients can be obtained as $D(BaCl_2)=1.39\times10^{-5}$ cm^2/s, $D(SrCl_2)=1.34\times10^{-5}$ cm^2/s, and $D(Na_2SO_4)=1.23\times10^{-5}$ cm^2/s. In the nucleation zone, the diffusion phenomenon, in principle, is more complex as the diffusion coefficients in a system containing more than two ionic species become concentration dependent [12] and thus their values change as the species concentrations evolve in time. However, the Na^+ and Cl^- ions that remain in solution after the barite-celestite crystals precipitate should effectively maintain the electroneutrality of the solution, so that the diffusion coefficients in the nucleation zone should not be very different from the binary coefficients calculated above.

III. NUMERICAL SOLUTIONS OF PDEs

The equations were nondimensionalized in the following way. The concentrations m_i were scaled by a typical value $\overline{m}\sim5$ mM$=5\times10^{-6}$ mole/cm^3. The solid phase concentrations were scaled by the inverse molar volume of $BaSO_4$ $\overline{c}$

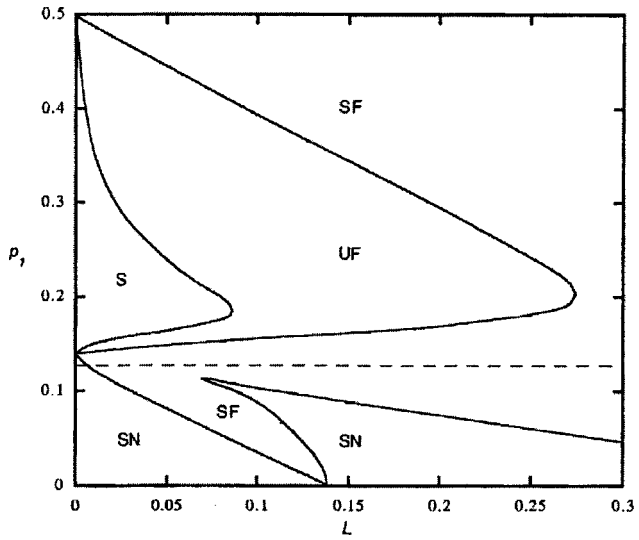

FIG. 2. Linear stability diagram for the reduced model of Ref. [9]. The corresponding parameter values are $\hat{m}_i=2$, $\alpha=0.89$, $\beta=1$, $d_B=0.79$, $d_C=0.74$, and $p_1=p_2$. The stability regions are denoted as follows: SF, stable focus; UF, unstable focus; *S*, saddle; and SN, stable node. The bistability region extends below the dashed line in the diagram. Reprinted from Ref. [9], with permission from Elsevier Science.

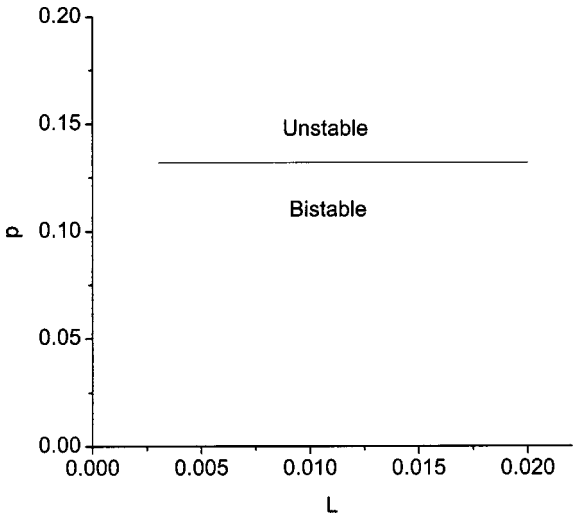

FIG. 3. Stability diagram for the full PDE model in one dimension. The stability of the steady state was determined numerically. For simplicity, here $d_B=d_C=1$, $p_1=p_2=p$, $\gamma=0$, $\alpha=1$, and $\beta=1$. The horizontal boundary between the stable and unstable regions corresponds to the line between the SF and UF regions in Fig. 2. The stability of the system for small values of L could not be determined because of the strong dependence on the width of the boundary layer l, which appears in numerical simulations when the concentration profile in the solution evolves on a spatial scale comparable with the size of the simulation grid.

$=1/v_{BA}=0.019$ mole/cm^3. The growth velocity was scaled by a typical value $\overline{V}\sim 10^{-8}$ cm/s, which was estimated by dividing the typical crystallite size by the duration of the experiment. The space coordinate x was scaled by the width of the diffusion boundary layer defined in Eq. (21): $\overline{l}=\overline{m}D_A/\overline{Vc}\approx 3$ mm where D_A is the effective diffusion coefficient for SO_4^{2-}, $D_A=1.23\times 10^{-5}$ cm^2/s. This value of the diffusion boundary layer width is consistent with the value obtained in Ref. [13] where the diffusion profile was similarly approximated by a linear segment in modeling calcite zoning. The time variable was scaled by $\overline{t}=\overline{l}^2/D_A\approx 8.3\times 10^3$ s$=2.3$ h and the effective crystal-solution interface width L was expressed in units of the characteristic zoning width $\overline{L}=\overline{Vt}\approx 0.8$ μm. In addition, several other dimensionless parameters were introduced: $\alpha=v_{CA}/v_{BA}$, $\beta=\beta'_{CA}/\beta'_{BA}$, $d_B=D_B/D_A$, and $d_C=D_C/D_A$. Equations (1)–(3), and (10) then transform into

$$\frac{\partial m_i}{\partial t}=d_i\frac{\partial^2 m_i}{\partial x^2}+\gamma V\frac{\partial m_i}{\partial x}, \tag{28}$$

$$m_i(l,t)=\hat{m}_i(t), \tag{29}$$

$$d_i\frac{\partial m_i}{\partial x}\bigg|_{x=0}+[m_i(0,t)\gamma-c_i(t)]V=0, \tag{30}$$

$$L\alpha\frac{dX}{dt}=[V_{BA}-X(V_{BA}+V_{CA}/\alpha)][X+(1-X)\alpha]^2, \tag{31}$$

where all the variables are in their dimensionless form and $d_A=1$. The ratio of the concentration scales in the aqueous and solid phases is $\gamma=\overline{m}/\overline{c}=2.5\times 10^{-4}$. Due to the finite grid size, the boundary condition (29) is taken at the distance l from the interface, which is of the order of $\overline{l}$.

The nondimensionalized system of three partial differential equations (28) alone with the boundary conditions (29) and (30) and the ordinary differential equation (31) were solved using a Crank-Nicholson algorithm with adaptive step size and iteration over the nonlinear term containing the growth velocity V.

First, crystal growth was considered for constant bulk species concentrations $\hat{m}_i=$const. For a one-dimensional system, due to the finite spatial extent of the system, a steady crystal growth regime is eventually achieved if the system is let to evolve for a sufficiently long time, in accordance with our analysis. The stability of these steady-state solutions can be investigated in analogy with the types of solutions found for the reduced version of the system [9]. In that paper, the linear stability analysis indicated the presence of a stable focus, an unstable focus, a stable node, and a saddle (Fig. 2). A bistable regime for which two different stable steady states coexist was observed for small values of the parameters p_1 and p_2.

Here, the stability of the steady state was determined numerically by observing the dynamical solution behavior in the vicinity of the steady state. Due to the difficulties in determining the correct type of linear stability for the numerical solutions, only the stability property (stable or unstable) for the steady state was recorded. The regions of stability found in the present case are illustrated in Fig. 3 for a simplified version of the system with $d_B=d_C=1$, $p_1=p_2=p$, $\gamma=0$, $\alpha=1$, and $\beta=1$. The bulk concentrations in the

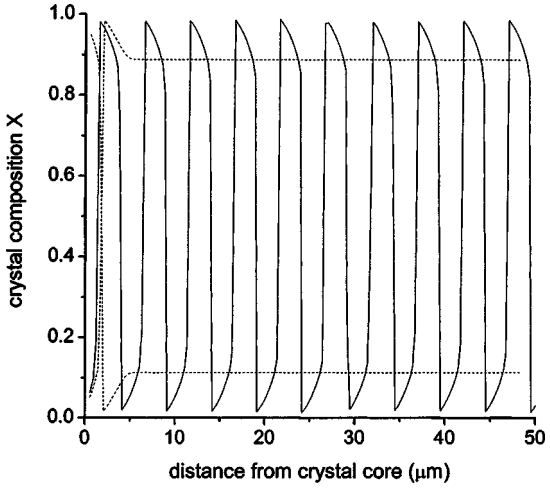

FIG. 4. Numerical solutions of the full PDE system for the growth of a flat crystallite face. The parameters are $d_B=d_C=1$, $p_1=p_2=p$, $L=0.01$, $\gamma=0$, $\alpha=1$, and $\beta=1$. The dashed lines are the solutions in the region of bistability in Fig. 3 for two different initial conditions with $p=0.13$. The solid line is the oscillatory solution for $p=0.14$. The bulk concentrations are considered constant $\hat{m}_i=2$.

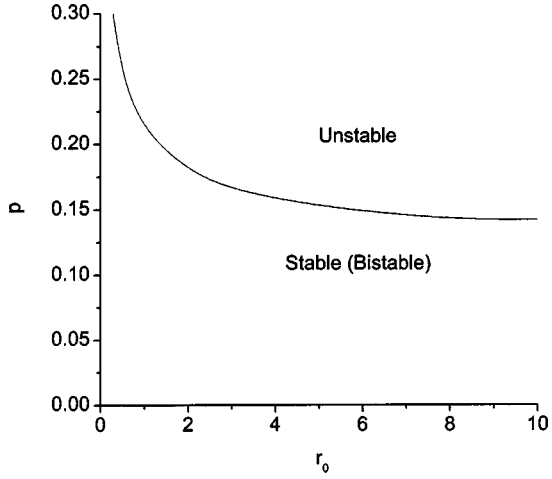

FIG. 5. Stability diagram for the full PDE model for a spherical crystallite. The stability of the system (obtained numerically) is indicated as a function of the initial crystallite radius r_0. The dimensionless interface roughness is $L=0.01$ and other parameter values are the same as in Fig. 3.

solution were taken as $\hat{m}_i=2$. For the range of the parameters L and p considered, two stable steady states coexist for small values of p (Fig. 4). For large values of p, the steady state is unstable and the numerical solution exhibits oscillatory character (Fig. 4). The exact value of p for which the steady state loses its stability depends on the value of l. The line that separates the regions of stability in Fig. 3 corresponds to the line that separates the regions of unstable focus and stable focus in Fig. 2. In the general case of arbitrary values of d_B, d_C, γ, α, and β, the region of bistability in Fig. 3 is separated from the region where the steady state becomes unstable by a region where there exists only one stable steady state. This is also consistent with the stability properties of the reduced system shown in Fig. 2. Increasing the values of the bulk concentrations shifts the curve in Fig. 3 down, thus enlarging the region where the steady state is unstable. In the general case of arbitrary d_B, d_C, γ, α, and β, the curve, which separates the region where a single stable steady state exists from the unstable region, is also shifted downward.

Similar results are obtained for the case of a spherical crystallite growth in the limit of large crystallite radius. For $r\sim 1$, the concentration in the solution varies on a spatial scale of the order $\overline{l}$ and the approximation of a flat crystal surface is sufficiently accurate. For smaller crystallites, however, the concentration variations occur on a much smaller scale and the system's dynamics is different (Fig. 5). For small initial crystallite radius, the stable steady state loses its stability only for large values of the parameter p.

To compare the simulated crystal composition profiles with the ones observed in the experiment, changes in the bulk solution concentrations need to be taken into account. Calculations based on Eqs. (16) indicate that concentrations $\hat{m}_i$ may change by as much as a factor of 10 during the crystal growth time.

The spatial concentration profiles calculated according to Eqs. (16) were verified to fit the experimental concentration data. The fit is satisfactory when the diffusion coefficient is chosen as $D_B=1.39\times 10^{-5}$ cm^2/s and the concentrations $M_{A,B,C}$ are taken in the gel at a position immediately adjacent to the reservoirs.

The calculated aqueous concentrations values at the crystallization site at the time of nucleation are shown in Table I for the cases in which the location of the nucleated crystallites is known from the $BaSO_4$ growth experiments in the same setup. The initial (core) composition of the observed crystallites [6] is also listed in Table I.

Figure 6 shows the types of numerical solutions obtained for the case of the growth of a spherical crystallite when the time dependence of the bulk concentrations in the solution is taken into account. The crystal composition X is shown as a function of the distance $r-r_0$. For sufficiently large initial crystallite size r_0, a transition from a stable steady state (either Ba rich or Sr rich) to an oscillatory solution occurs as the supersaturation in the solution increases due to the solute diffusion from the reservoirs [Fig. 6(a)]. The same type of dynamical behavior is obtained when the growth of a flat infinitely large crystal face is considered. For smaller crystallites, however, this transition occurs for higher values of the local solution concentrations (greater time t counted from the start of the experiment) [Fig. 6(b)].

Due to the difference in the diffusion coefficients, molar volumes, and kinetic coefficients of the two solid solution end members, one of the two stable steady states may lose its stability while another remains stable as the solution concentrations increase with time. In this case, the crystal composition may jump rapidly from one composition range to another [Figs. 6(c) and 6(d)]. Further increase in the local supersaturation may cause a subsequent transition to an oscillatory type of solution [Fig. 6(d)].

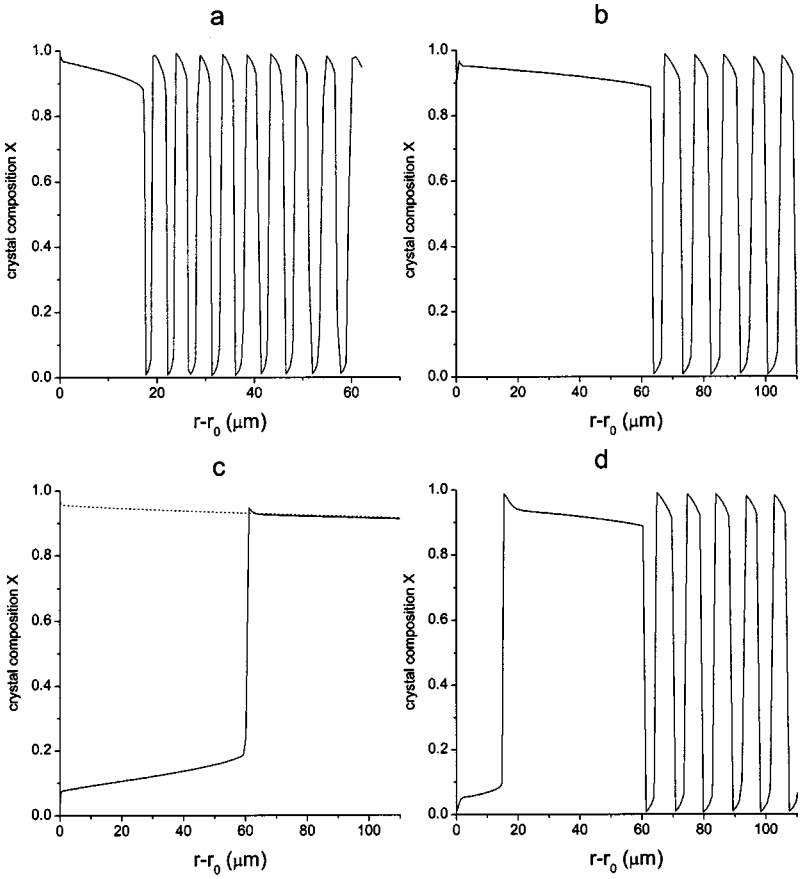

FIG. 6. Numerical solutions of the full PDE system for a spherical crystallite. The crystal composition X is shown against the radial distance $r-r_0$, which characterizes the amount by which the crystal has grown beyond its initial size r_0. The time dependence of the bulk solution concentrations is considered according to Eq. (16), the values of the reservoir concentrations M_i are given below along with the time t counted from the moment the solutions enter the gel column to the moment the crystal radius is r_0. Other parameter values are $d_B=1.127$, $d_c=1.087$, $p_1=0.08$, $p_2=0.10$, $\alpha=0.89$, $\beta=0.9$, $\gamma=2.5\times10^{-4}$, and $L=0.01$. The growing crystallite was considered to be located at $y=15$ cm from the reservoir containing $BaCl_2$ and $SrCl_2$ (a) $r_0=10$, $M_i=0.5M$, $t=300$ h; for larger r_0, the result is about the same, which corresponds to the approximation of a flat crystallite surface. (b) $r_0=3.0$, $M_i=0.5M$, $t=400$ h; (c) $r_0=0.5$, $M_i=0.3M$, $t=360$ h; (d) $r_0=3.0$, $M_i=0.5M$, $t=400$ h.

IV. REDUCED MODEL

As was shown in the preceding section, the species concentrations in the solution vary almost linearly with the distance from the crystal-solution interface. This diffusion profile can be approximated by a single straight line, in which case the model can be reduced to a system of coupled ordinary differential equations for the concentrations at the crystal face $m_i(0,t)$ [9]. Such reduction allows one to perform a linear stability analysis and thus analytically obtain the qualitative characteristics of the system's dynamics.

Equations (28) are integrated over x and the boundary conditions (29) and (30) are taken into account. Using dimensionless variables and omitting the argument $(0,t)$ from m_i, equations (28)–(30) then become [9]

$$\frac{dm_A}{dt}=2(\hat{m}_A(t)-m_A)+2V[\gamma\hat{m}_A(t)-c_A]-\frac{d\hat{m}_A(t)}{dt},$$

$$\frac{dm_B}{dt}=2d_B[\hat{m}_B(t)-m_B]+2V[\gamma\hat{m}_B(t)-c_B]-\frac{d\hat{m}_B(t)}{dt}, \tag{32}$$

$$\frac{dm_C}{dt}=2d_C[\hat{m}_C(t)-m_C]+2V[\gamma\hat{m}_C(t)-c_C]-\frac{d\hat{m}_C(t)}{dt},$$

where $c_A=c_B+c_C$ and c_B and c_C are defined in Eq. (8). Equation (31) completes the reduced model. This set of equations constitutes the version of the model investigated in Ref. [9].

In the case of a spherical crystal, a similar reduction of Eqs. (4)–(6) to a system of ODEs involves integration of equation (4) over volume and approximating the diffusion profile by a linear segment of length l. The resulting system of equations in a nondimensionalized form is

$$\begin{aligned}\frac{dm_i}{dt}&\left(\frac{l^3}{12}+\frac{rl^2}{3}+\frac{r^2l}{2}\right)\\&=d_i[\hat{m}_i(t)-m_i]\frac{(l+r)^2}{l}\\&\quad-r^2V[c_i-\gamma m_i(t)]-\gamma m_iV\left(\frac{l^2}{3}+rl\right),\\&\quad-\gamma\hat{m}_iV\left(\frac{2l^2}{3}+rl\right)+\gamma V[\hat{m}_i(t)-m_i]\frac{(l+r)^3-r^3}{3l}\\&\quad-\frac{d\hat{m}_i(t)}{dt}\left(\frac{l^3}{4}+\frac{2rl^2}{3}+\frac{r^2l}{2}\right),\end{aligned} \tag{33}$$

where r is the radius of the crystal, which slowly increases as

$$r(t)=r(0)+\gamma\int_0^t V(t')dt'. \tag{34}$$

The width of the diffusion boundary layer l, in general, varies with r. This dependence may be approximated, for example, by choosing the value of l to correspond to the

distance from the crystal surface where the solution concentration (23) for SO_4^{2-} is equal to $(1-\varepsilon)\hat{m}_A$, where ε is a small parameter. This gives

$$l = r\left(\frac{Vr}{v_{BA} d_A \varepsilon \hat{m}_A} - 1\right). \tag{35}$$

These reduced models (31) and (33) reproduce the general features of the dynamics of the original PDE model. It is therefore useful in investigating the system's behavior for small crystal radius r where the PDE equations become stiff. Also, it allows the investigation of the system's dynamic properties by means of a straightforward linear stability analysis.

The linear stability analysis for the system of equations (32) and (31) describing the growth of a flat crystallite surface was performed in Ref. [9] and its main results are summarized in the stability diagram of Fig. 2. Equations (33) reduce to Eq. (32) in the limit of large r (and $l=1$) and therefore their stability properties are the same in that limit. However, as was shown earlier [e.g., Eq. (23)], the crystal growth mechanism depends on the crystallite size. Therefore, it is important to investigate how the stability of the system changes with the crystallite radius r and the width of the diffusion boundary layer l.

Assuming that r and l change slowly, a pseudo-steady-state for the autonomous ($\hat{m}_i = \text{const}$) version of the equations can be obtained by setting the left-hand side of Eqs. (33) to zero. If the terms proportional to γ are neglected for simplicity, the steady state is easily shown to have the form

$$m_{i,\mathrm{st}} = \hat{m}_i - \frac{V_{\mathrm{st}} c_{i,\mathrm{st}}/d_i}{l/r^2 + 2/r + 1/l}, \tag{36}$$

where V_{st} is the steady state growth rate. In the limit of large $r (r \gg l)$ it reduces to

$$m_{i,\mathrm{st}} \approx \hat{m}_i - c_{i,\mathrm{st}} \frac{V_{\mathrm{st}}}{d_i} l, \tag{37}$$

which is consistent with Eq. (22) evaluated at $x=l$.

The solution of the system of nonlinear equations defined by Eqs. (36) and Eq. (31) (with the left-hand side equal to zero) was found numerically to obtain the steady-state values of $m_{i,\mathrm{st}}$ and X_{st}. A linear stability analysis was then performed. The stability of the steady states was investigated by finding the eigenvalues of the Jacobian matrix of the systems (33) and (31) for each steady state.

For a wide range of parameters, there exist three steady states for which the crystal composition is close to the values in the set (26). In the calculations, the terms proportional to γ were neglected, and the following simplifications were made: $p_1 = p_2$, $\beta = 1$, and $d_A = d_B = d_C = 1$. With this choice, the steady states for which the crystal is Ba rich and Sr rich are symmetric in crystal composition and have exactly the same stability properties while the crystal composition in the third steady state is exactly $X^* = 0.5$.

The steady state $X^* = 0.5$ was unstable for all values of the parameters considered. A typical stability diagram for the steady state for which the crystal is Ba rich (or Sr rich) is shown in Fig. 7. The stability diagram indicates that the steady state may become unstable via a Hopf bifurcation as the crystallite radius and the width of the diffusion boundary layer [Eqs. (34) and (35)] increase. This result suggests that an autocatalytic oscillatory crystal growth may occur for given bulk solution concentrations when the size of the crystallite exceeds a certain critical value.

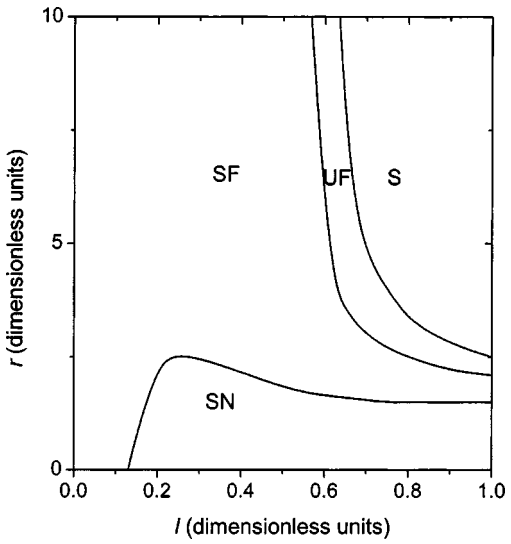

FIG. 7. Linear stability diagram for the reduced model of a spherical crystal. The stability properties are shown for either one of the two steady states, where X is close to 0 or 1. The dimensionless parameter values are $\hat{m}_i = 3$, $d_B = d_C = 1$, $p_1 = p_2 = 0.20$, $L = 0.01$, $\alpha = \beta = 1$, and $\gamma = 0$. The notation of the stability regions is the same as in Fig. 2.

Increasing the bulk solution concentrations $\hat{m}_i$ generally shifts the curves in Fig. 7 towards smaller values of the crystallite radius, thus decreasing the critical value of the crystallite radius for which the steady state loses its stability.

V. NUMERICAL SOLUTION OF THE REDUCED MODEL

The numerical solutions of the reduced model for the growth of a spherical crystallite are illustrated in Fig. 8. Equations (31) and (33) were solved using a fourth-order Runge-Kutta algorithm and the integral (34) was calculated using the trapezoidal rule.

First, the dynamics of the system was studied for constant bulk concentrations. For small crystallite radius, the system quickly settles into one of the stable steady states (either Ba rich or Sr rich). Switching from one steady state to another is possible as the crystal size r and correspondingly the width of the diffusion boundary layer increase slowly in time [Fig. 8(a)]. For large crystallite size, oscillatory solutions similar to the solutions generated by the full PDE model are found (Figs. 8(b) and 8(c)].

When the time dependence of the bulk concentrations (16) is considered, transitions between the steady states can be obtained similarly to the ones observed for the PDE model as the concentrations in the solution around the growing crystallite evolve in time. The steady-state solution of the

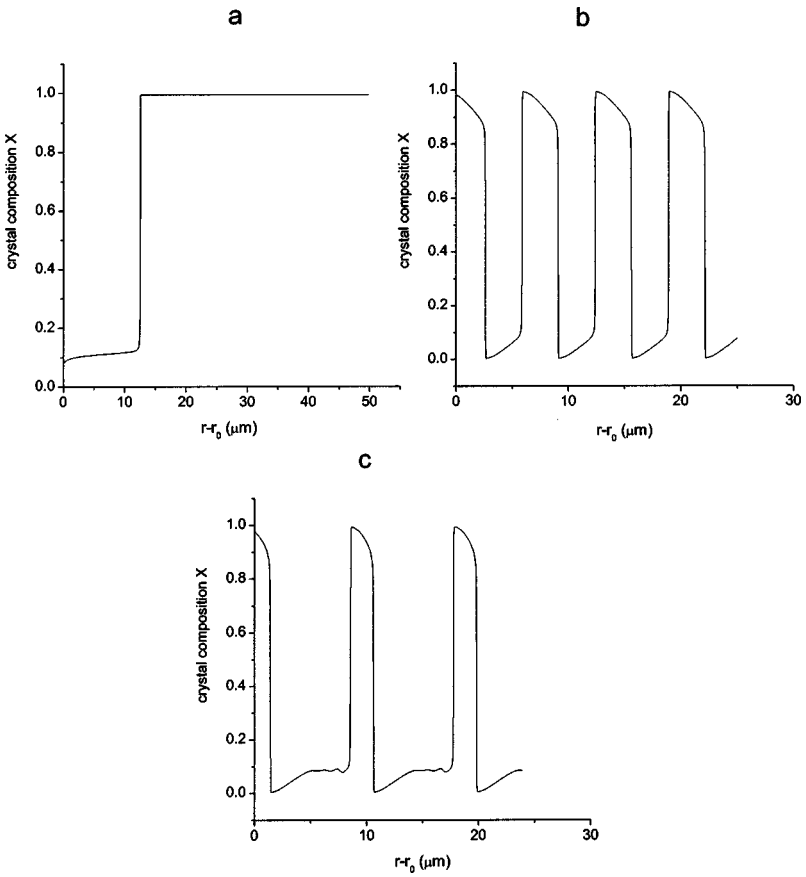

FIG. 8. Compositional profile generated by the reduced model for a spherical crystal. The bulk solution concentrations were kept constant and the parameter values were $d_B=1.127$, $d_c=1.087$, $L=0.01$, $\alpha=1.0$, $\beta=0.9$, and $\gamma=2.5\times10^{-4}$. (a) A change in the crystal composition occurs as the crystal grows larger as a result of the $l(r)$ dependence. $\hat{m}_A=2.7$, $\hat{m}_B=3.6$, $\hat{m}_C=2.7$, $p_1=0.15$, $p_2=0.11$, $\varepsilon=0.01$, and $r_0=0.25$. (b) Oscillatory solution corresponding to the saddle region (analogous to that shown in Fig. 7) for very large crystal size. $\hat{m}_A=5.0$, $\hat{m}_B=3.1$, $\hat{m}_C=2.9$, $p_1=0.09$, $p_2=0.13$, $l=1.0$, and $r_0=10$. (c) Solution that roughly corresponds to the border region between the unstable focus and the saddle region (analogous to the UF and *S* regions in Fig. 7). The parameter values are the same as in (b), with the exception of $p_2=0.15$.

system, in many cases, sensitively depends on the bulk solution concentrations and therefore on the location of the growing crystallites in the gel column. Relatively small variations in the concentration values lead to qualitative changes in the type of solution, such as transition from a steady state characterized by a Sr-rich crystal composition to a steady state where the crystal is Ba rich. Typically, only one such transition can be numerically observed in the course of the crystal growth with the bulk concentrations time dependence described by Eqs. (16).

The value of the crystallite radius for which the steady state loses its stability for the bulk solution concentrations and the parameter values used here is greater than the typical crystallite size observed in the experiments by about an order of magnitude. However, switching between the stable steady states, which results in an oscillatory zoning pattern, can be observed in the framework of the current model when small random fluctuations of the bulk concentrations of species at the crystal nucleation site are considered.

VI. THE EFFECTS OF NOISE

The effect of small fluctuations in the solution concentrations can be considered in the full PDE model by adding a stochastic term to the deterministic bulk concentrations (16).

$$\hat{m}_i(t)=\hat{m}_{i\,0}(t)+\sigma_i\eta_i(t), \tag{38}$$

where $\hat{m}_{i\,0}(t)$ are the bulk concentrations of the salts in the solution, $\eta_i(t)$ are the respective noise processes, and the parameters σ_i describe the noise amplitude. The fluctuations in the solution concentrations around the crystallite may result, for example, from disturbances caused by the growth of other crystallites. From physical considerations, the noise processes $\eta_i(t)$ are expected to be approximately stationary. An Ornstein-Uhlenbeck noise [14] with zero mean and unit variance is therefore used to simulate the aqueous concentration fluctuations for all species. The correlation time τ_n for the noise processes is chosen significantly larger than the time step in the numerical calculations but much smaller than the total crystal growth time. Since the electroneutrality of the solution can be maintained by the corresponding fluctuations in the Na^+ and Cl^- aqueous concentrations, the noise processes for all three species of interest can be considered relatively independent from each other.

When the stochastic bulk concentrations (38) are considered in the full PDE model (28)–(31) for the growth of a flat crystal face, an interesting noise-induced effect can be observed when the parameters are chosen to correspond to the bistable region in the stability diagram of Fig. 3 but close to the instability line. Hence, deterministically, two stable steady states coexist for the given choice of parameters. In the presence of noise, however, fluctuations in the bulk concentrations may induce the system to make a temporary transition from the bistable region of its phase space to the unstable region (Fig. 3 or 5). This results in stochastically induced oscillatory compositional patterns [Fig. 9(a)] characterized by variations of the crystal composition over a wide range.

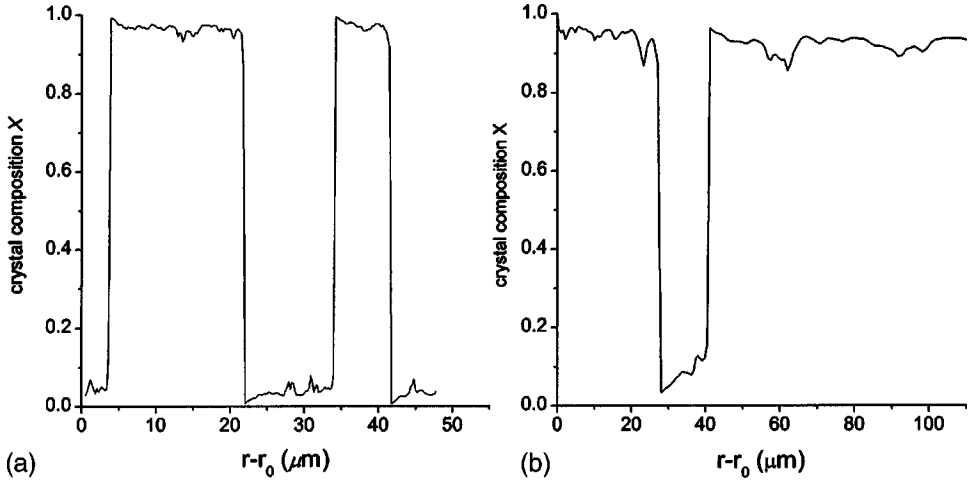

FIG. 9. The effect of noise on the full PDE model. For the parameter values chosen, two stable deterministic steady states coexist. (a) Oscillatory zoning compositional profile generated by the model for the case of a flat crystallite surface. $\hat{m}_i=2$, $d_B=1.127$, $d_C=1.087$, $p_1=p_2=0.10$, $\alpha=0.89$, $\beta=0.9$, $\gamma=2.5\times10^{-4}$, $L=0.007$, and $l=2$. Independent Ornstein-Uhlenbeck noise processes with amplitudes $\sigma_i=0.3$ and noise correlation time $\tau_n=0.1$ are used to simulate fluctuations in the bulk concentrations. (b) Ba-Sr-Ba type of zoning generated by the model for the case of a spherical crystallite. $M_i=0.3M$, $d_B=1.127$, $d_C=1.087$, $p_1=p_2=0.17$, $\alpha=0.89$, $\beta=0.9$, $\gamma=2.5\times10^{-4}$, $L=0.01$, $t=360$ h, $y=15$ cm, and $r_0=0.5$. Ornstein-Uhlenbeck noise parameters are $\sigma_i=0.3$ and $\tau_n=2.0$. Relatively large τ_n may describe fluctuations caused, for example, by the growth of other crystallites in the gel.

The same type of noise-induced oscillations is also observed for the PDE model for the growth of a spherical crystallite [Fig. 9(b)]. The frequency of these noise-induced events depends on the noise amplitude and correlation time as well as on how far the system is from the unstable region in its parameter space. Thus, for small supersaturations, in the presence of relatively small noise, only one or two rapid crystal composition changes may occur during the crystal growth time. This results in the Ba-Sr, Sr-Ba, Ba-Sr-Ba, or Sr-Ba-Sr types of zoning (see Table I). For higher supersaturations (higher reservoir solution concentrations), these noise-induced concentration changes are more frequent, which results in noisy oscillatory zoning.

VII. CONCLUSION

The present model of oscillatory zoning in $(Ba,Sr)SO_4$ solid solution by an autocatalytic mechanism generates solutions that are qualitatively consistent with the observations of the experimentally grown crystals. Consideration of the physical parameters that determine the crystal growth mechanism as well as the linear stability analysis of the reduced model for the growth of a spherical crystallite indicate that oscillatory zoning arises due to the distortion of the diffusion concentration profiles in the solution caused by the increase in the crystallite size. The oscillatory zoning occurs when the concentrations of the salts in the solution are large and the crystal growth proceeds at a fast enough rate to impact the diffusion profiles in the solution around the crystallite. Fluctuations in the crystallite growth environment may be a significant factor contributing to the oscillatory zoning formation as they facilitate transitions between the steady states of the dynamical reaction-diffusion system.

ACKNOWLEDGMENTS

The authors would like to thank the Natural Science and Engineering Research Council of Canada and the Ministry of Training, Colleges and Universities of Ontario for financial support.

APPENDIX

In this appendix we derive the differential equation for the evolution of the kinetically defined composition at the surface of a spherical crystal [Eq. (10)]. We proceed in the spirit of Ref. [15], where a similar derivation was performed for the case of a flat interface. We consider an atomically rough surface of a spherical crystallite, which is a binary solid solution with the end-members B and C, in contact with a supersaturated solution. If the number of the atomic units of elements B and C in the crystallite surface are n_B and n_C, respectively, then the surface molar composition X is defined by

$$X=\frac{n_B}{n_B+n_C}. \tag{A1}$$

Let us define the interface as a thin spherical shell, whose width is of the order of the length scale of the crystal surface fluctuations. The characteristic radius of this shell r can be used as the average radius of the crystallite. If the accretion rates V_B and V_C are defined as the rates (length/time) of crystal surface growth (or dissolution) due to the arrival (departure) of the units of B and C, respectively, then the incoming fluxes of the units of B and C to the interface are given by

$$\frac{\partial n_B^{\text{in}}}{\partial t} = G_B 4\pi r^2 = V_B \frac{4\pi r^2}{v_B}, \quad \frac{\partial n_C^{\text{in}}}{\partial t} = G_C 4\pi r^2 = V_C \frac{4\pi r^2}{v_C}, \tag{A2}$$

where G_B and G_C are the molecular fluxes (number of molecular units per unit area per unit time) towards the crystallite surface and v_B and v_C are the atomic volumes of the species. While the units are arriving from the solution to the outer surface of the interface shell, they are leaving the shell at its inner surface due to the motion of the shell associated with the crystallite growth. The corresponding outgoing molecular flux is proportional to the surface composition X and the surface area:

$$\frac{\partial n_B^{\text{out}}}{\partial t} = X 4\pi r^2 K, \tag{A3}$$

where K is a coefficient of proportionality. In the steady growth regime, when the number of B units in the interface shell does not change, the change in the number of incoming B units per unit time is balanced by the change in the number of outcoming B units. At the same time, the surface composition X corresponding to this steady growth regime may be defined kinetically [10] through the incoming fluxes G_B and G_C as

$$X_{\text{st}} = \frac{G_B}{G_B + G_C}. \tag{A4}$$

By comparing Eqs. (A3) and (A4) it follows that $K = G_B + G_C$ and

$$\frac{\partial n_B^{\text{out}}}{\partial t} = X 4\pi r^2 \left(\frac{V_B}{v_B} + \frac{V_C}{v_C} \right). \tag{A5}$$

Let us now define the molecular density in the solid at the interface as

$$\rho = \frac{1}{X v_B + (1-X) v_C}. \tag{A6}$$

The number of B units in the interface shell may be then obtained as

$$n_B = 4\pi r^2 \rho X L, \tag{A7}$$

where the parameter L (assumed constant) is the effective width of the rough crystallite-solution interface defined as

$$L = \frac{1}{4\pi r^2} \int_{\text{shell}} \theta(\vec{r}\,'; t) d^3 \vec{r}\,', \tag{A8}$$

where the function θ is equal to 1 if the point $\vec{r}\,'$ is located in the solid and zero otherwise. The total change in the number of B units in the interface is then

$$\frac{\partial n_B}{\partial t} = \frac{\partial}{\partial t}(4\pi r^2 \rho X L) = L \frac{\partial}{\partial t}(\rho X) + 8\pi r L \rho X \frac{\partial r}{\partial t}. \tag{A9}$$

By equating this expression to the difference between the incoming flux (A2) and the outgoing flux (A5) and using the expression (A6) for ρ, one obtains

$$\frac{L\alpha}{[X + (1-X)\alpha]^2} \frac{dX}{dt} + \frac{2L}{r} \frac{X}{X + (1-X)\alpha} \frac{\partial r}{\partial t} = V_B - X\left(V_B + \frac{V_C}{\alpha} \right), \tag{A10}$$

where $\alpha = v_C / v_B$. Taking into account that [16]

$$\frac{\partial r}{\partial t} \approx V_B + V_C \tag{A11}$$

and that $L \ll r$, the term containing $2L/r$ may be neglected with respect to the last term on the right-hand side of Eq. (A10) and we recover equation (10):

$$L\alpha \frac{dX}{dt} = [V_B - X(V_B + V_C/\alpha)][X + (1-X)\alpha]^2. \tag{A12}$$

[1] M. Shore and A. D. Fowler, Can. Mineral. **34**, 1111 (1996).
[2] A. M. Turing, Philos. Trans. R. Soc. London, Ser. B **237**, 37 (1952).
[3] A. Putnis, L. Fernandez-Diaz, and M. Prieto, Nature (London) **358**, 743 (1992).
[4] M. Prieto, A. Putnis, and L. Fernandez-Diaz, Geol. Mag. **130**, 289 (1993).
[5] M. Prieto, A. Putnis, and L. Fernandez-Diaz, Geol. Mag. **127**, 485 (1990).
[6] M. Prieto, A. Fernandez-Gonzalez, A. Putnis, and L. Fernandez-Diaz, Geochim. Cosmochim. Acta **61**, 3383 (1997).
[7] A. Putnis, M. Prieto, and L. Fernandez-Diaz, Geol. Mag. **132**, 1 (1995).
[8] C. M. Pina, M. Enders, and A. Putnis, Chem. Geol. **168**, 195 (2000).
[9] I. L'Heureux and B. Jamtveit, Geochim. Cosmochim. Acta **66**, 417 (2002).
[10] D. Stauffer, J. Aerosol Sci. **7**, 319 (1976).
[11] I. Markov, *Crystal Growth for Beginners. Fundamentals of Nucleation, Crystal Growth and Epitaxy* (World Scientific, Singapore, 1995).
[12] A. C. Lasaga, *Kinetic Theory in the Earth Sciences* (Princeton University Press, Princeton, 1998).
[13] Y. Wang and E. Merino, Geochim. Cosmochim. Acta **56**, 587 (1992).
[14] C. W. Gardiner, *Handbook of Stochastic Methods for Physics, Chemistry and the Natural Sciences* (Springer-Verlag, Berlin, 1983).
[15] P. Ortoleva, *Geochemical Self-Organization*, Oxford Monographs on Geology and Geophysics Ser., Vol. 23 (Oxford University Press, New York, 1994).
[16] I. L'Heureux, Phys. Rev. E **62**, 3234 (2000).